Supporting Information for "" The shelf-to-basin transport of iron from the Northern U.S West Coast to the Pacific Ocean"

Anh Le-Duy Pham[1*], Pierre Damien[1] *, Daniel McCoy[1], Matthew Mar[1],

Fayçal Kessouri[2], James C McWilliams[1], James Moffett[3], Daniele Bianchi[1]

[1]Department of Atmospheric and Oceanic Sciences, University of California Los Angeles, Los Angeles, CA, USA

[2]Southern California Coastal Water Research Project

[3]Department of Biological Sciences, University of Southern California, Los Angeles, CA, USA

Contents of this file

---

*A.L.P. and P.D. contributed equally to this work

- Figure S4

2. Seasonal variability of the California Undercurrent

- Figure S5

3. Spatial variability of iron concentration offshore

- Figure S6

1. Model validation

1.1. Model validation: Iron

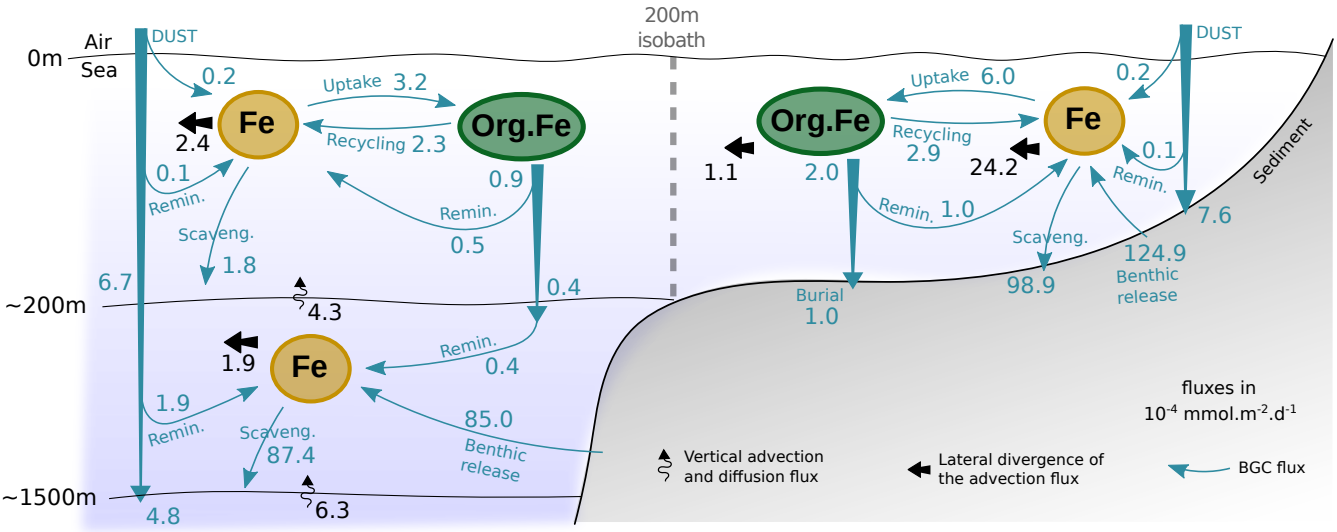

Figure S1. Budget analysis for the ocean Fe cycling along the Northern US West Coast (from Cape Mendocino to Vancouver Island) over a 9-year period from 2008-2016. Dark cyan arrows are biogeochemical fluxes; black curly arrow is vertical advection and diffusion; and black arrow is divergence of lateral advection. The boundary between coastal and open ocean areas is defined as the 200m isobath. In this figure, physical and biogeochemical terms are vertically integrated over a surface layer (0-200m) and a deep layer (200-1500m). All terms are expressed per unit area (10^{-4} mmol/m2/day) to facilitate the comparison of Fe cycling and transport terms between different regions of the domain. The transport terms are calculated as the divergence of horizontal and vertical fluxes, which, for vertical transport, include turbulent diffusion processes. Note that sedimentary dFe release in the offshore region occurs on the continental slope, where the average value is 727 10^{-4} mmol/m2/d. However, in order to represent a "closed" dFe budget (where sources and sinks balance), this figure reports the average terms normalized by the oceanic area extending up to 400 km offshore, thus much larger than the area of the continental slope, resulting in a lower average value.

Table S1. Sources of our dFe data compilation along with information on the type of Fe being measured

Data Sources	Iron Measurement Type
Landing and Bruland (1987)	dFe (0.3μm filter) and particulate Fe
Martin and Michael Gordon (1988)	dFe (0.4μm filter) and particulate Fe
Johnson et al. (2001)	dFe (0.45μm filter)
Johnson et al. (2003)	dFe (0.45μm filter)
Chase, van Geen, Kosro, Marra, and Wheeler (2002)	dFe (unfiltered, non acidified sample stream)
Fitzwater et al. (2003)	Dissolvable (Fe(III) detected after seawater is held at pH $\sim$ 3 for 1 min.) and particulate Fe
Firme, Rue, Weeks, Bruland, and Hutchins (2003)	dFe (0.2μm filter)
Chase et al. (2005)	Dissolvable Fe: Fe species passed through a 20μm filter and were acidified inline to pH 3.4 for 1 minute prior to analysis
Lohan and Bruland (2008)	dFe (0.4μm filter)
Elrod, Johnson, Fitzwater, and Plant (2008)	dFe (0.5μm filter). Dissolvable Fe is defined as Fe leached from particles at pH 3.2
Severmann, McManus, Berelson, and Hammond (2010)	dFe (0.45μm filter)
King and Barbeau (2011)	dFe (0.4μm filter)
John, Mendez, Moffett, and Adkins (2012)	dFe (0.45μm filter)
Biller, Coale, Till, Smith, and Bruland (2013)	dFe (0.2μm filter)
Bundy, Biller, Buck, Bruland, and Barbeau (2014)	dFe (0.2μm filter)
Bundy et al. (2015)	dFe (0.45μm filter)
Bundy, Barbeau, Carter, and Jiang (2016)	dFe (0.2μm filter)
Hogle et al. (2018)	dFe (0.4μm filter)
Boiteau et al. (2019)	dFe (0.2μm filter)
Till et al. (2019)	dFe (0.2μm filter)
Kelly et al. (2021)	dFe (0.2μm filter)
Wong, Nishioka, Kim, and Obata (2022)	dFe (0.2μm filter)
Abdala et al. (2022)	dFe (0.2μm filter)

1.2. Model validation: Oxygen

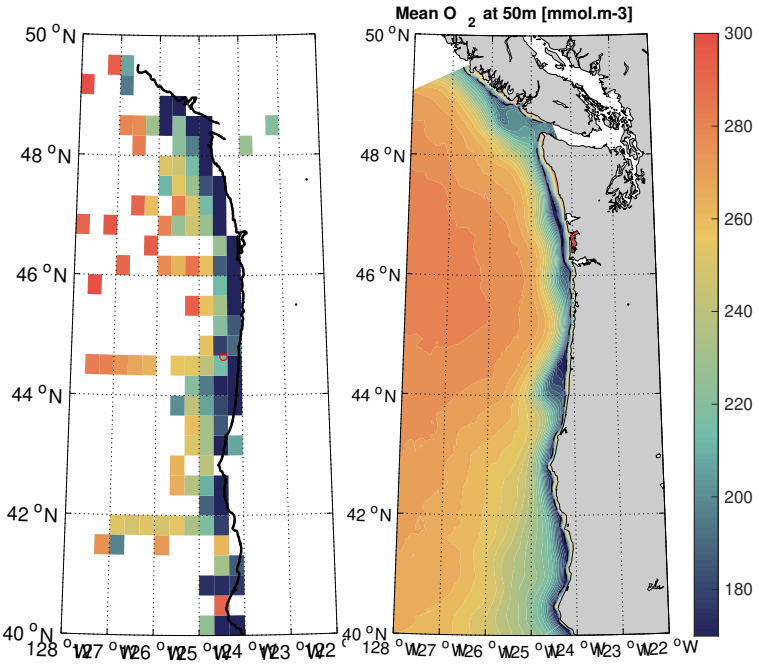

Figure S2. Maps of mean oxygen at 50m retrieved from (left) in-situ observations and (right) ROMS solutions from December 1999 to November 2017. Observations were collected from various sources and gridded at 1/3 degree resolution. For the rigth panel, the (dashed line) 50 m isobath is superimposed and, for waters shallower than 50 m, the mean oxygen field at bottom is shown. Taking into account that the lower mean oxygen concentration observed on the shelf is partially due to the larger amount of oxygen measurement during summer, the mean distribution of the modeled oxygen in ROMS is overall in good agreement with observed concentration.

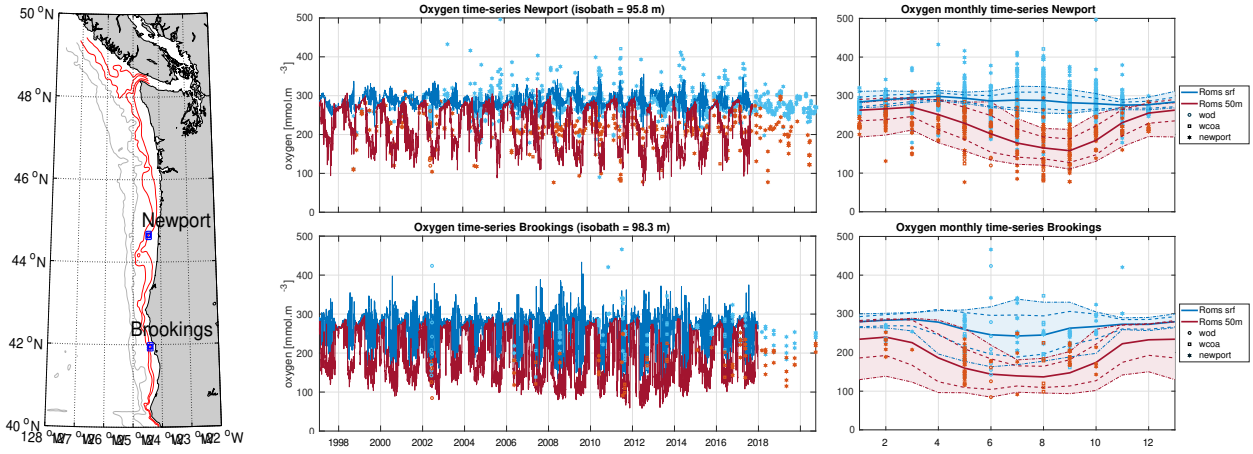

Figure S3. (Left panel) Location of the 2 geographical points selected for time-series comparisons in central and left panels. Red contours represents the 100 and 200m isobath that define the shelf and the grey contours are the 1000 and 2000 m isobath. (Central panels) Simulated (lines) and observed (dots) oxygen concentration time series at (upper) Newport and (lower) Brookings. The surface time series is displayed in blue and the 50m time series in red. For observations, each marker shape corresponds to a dataset source. We collected, compiled and merged data from the West Coast Ocean Acidification Cruises (WCOA) (Feely et al., 2016), the World Ocean Database (WOD) (Garcia et al., 2009), and the Newport hydrographic line (Risien et al., 2023). (right panels) Corresponding seasonal cycles with the (full line) mean, the (dashed line) daily rms and the (dots line) 5th and 95th percentiles of the monthly distribution. Despite an underestimation of the temporal variability evidenced by the wider spread of observations measurements, the seasonal oxygen variability is overall well reproduced.

1.3. Model validation: California Undercurrent

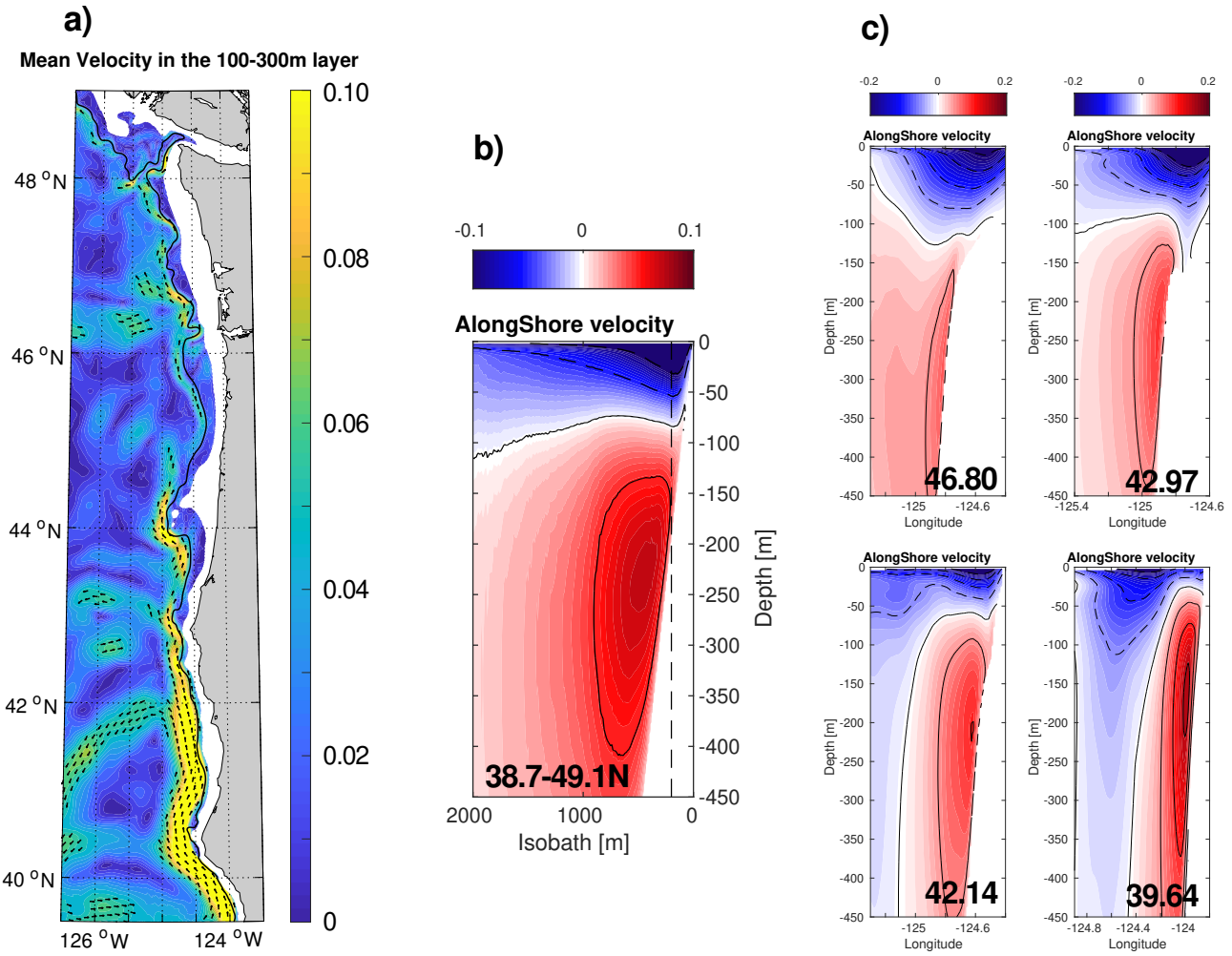

Figure S4. (a) Depth-averaged subsurface flow between 100 and 300 m in m/s. (b) Spatial mean section of alongshore flow between 38.7 and 49.1 °N, shown in an isobath/depth coordinate system. Positive verlocity are in the poleward direction. Black lines evidence velocity contours in steps of 0.05 m/s, the dashed line stand for negative alongshore velocity (or in the equatorward direction). (c) Selected sections of the alongshore flow. This figure compares the modeled CUC with the ADCP observations reported in Pierce et al. (2000). Panel a compares with figure 1, panel b with figure 3 and panel c with figure 2. Despite some differences likely related to the interannual variability of the CUC, the model velocity and position are overall within the range of the observations. Thus, the model produces a realistic CUC.

2. Seasonal variability of the California Undercurrent

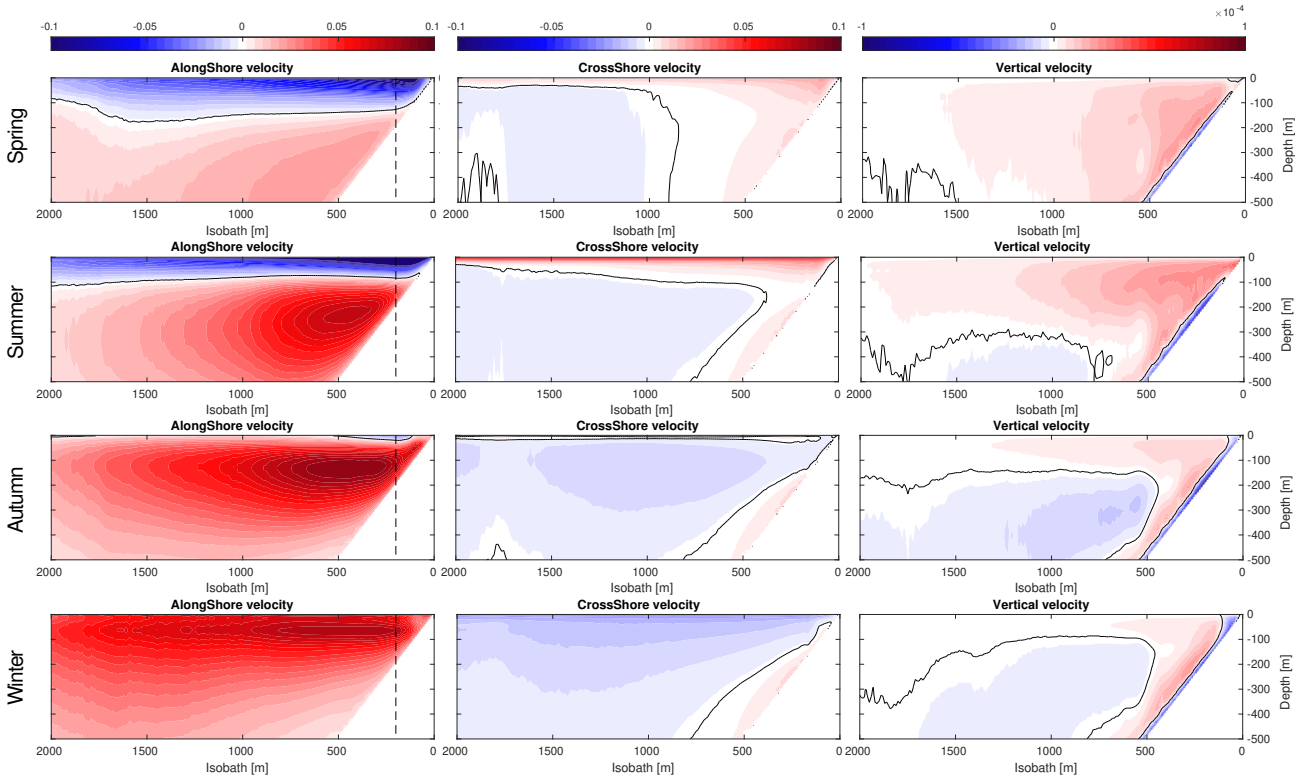

Figure S5. Seasonal variability of the nearshore flow shown in an isobath/depth coordinate system. Velocity were projected into the alongshore (positive directed poleward), crossshore (positive directed offshore), and vertical (positive directed upward) directions. Black line evidence the zero seasonal mean motion. The CUC is evienced by the subsurface alongshore velocity maximum (right panel). It is present throughout the whole year but intensified in Autumn. The CUC-topographic interaction produces an Ekman flow in the bottom mixed layer directed offshore (central panels) and downwrad (right panel). Similar to the CUC, this bottom-confined downhill flow is active during the whole year but intensified in Autumn.

3. Spatial variability of iron concentration offshore

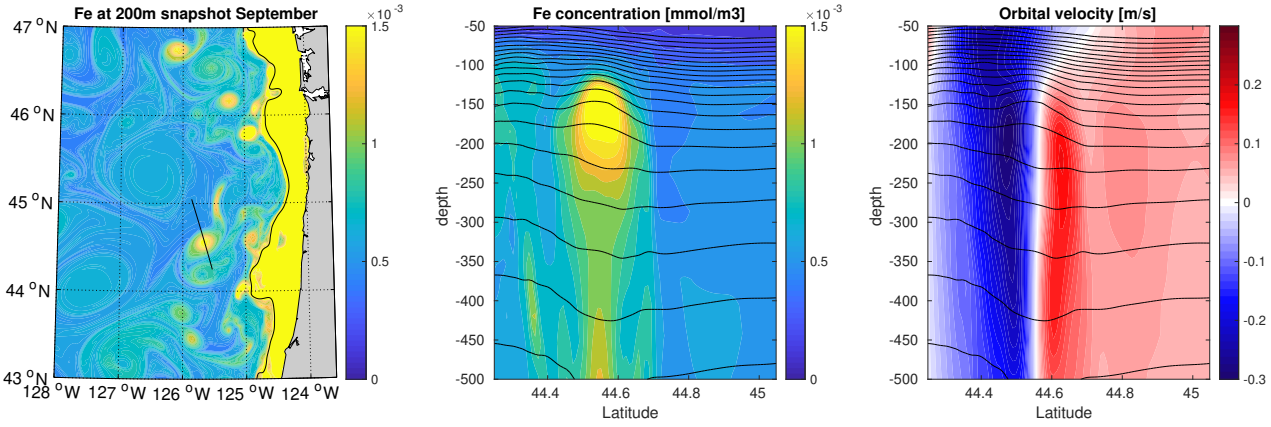

Figure S6. (a) Snapshot of the iron concentration at 200m depth in September. The black line highlights the 200m isobath and the bottom concentration is shown for depth shallower than 200m. Offshore, a significant amount of the iron released from the shelf is found in lenslike eddies characterized by a large positive iron anomaly. A crosssection (black transect on figure 1) of (b) iron and (c) velocity across one eddy evidences a subthermocline, low-stratified, and anticyclonic structure characteristic of the "Cuddies" described in Pelland et al. (2013). The large iron concentration in cuddies evidence the shelf origin of the water trapped in their cores where it undergoes mixing and stirring rates much lower than the background flow. This suggest Cuddies as a significant and effective mechanism for the iron shuttle from the shelf to remote offshore regions. This requires a closer inspection in future studies.

References

Abdala, Z. M., Clayton, S., Einarsson, S. V., Powell, K., Till, C. P., Coale, T. H., & Chappell, P. D. (2022). Examining ecological succession of diatoms in california current system cyclonic mesoscale eddies. *Limnology and Oceanography*, *n/a*(n/a). Retrieved from https://aslopubs.onlinelibrary.wiley.com/doi/abs/10.1002/lno.12224 doi: https://doi.org/10.1002/lno.12224

Biller, D. V., Coale, T. H., Till, R. C., Smith, G. J., & Bruland, K. W. (2013). Coastal iron and nitrate distributions during the spring and summer upwelling season in the central california current upwelling regime. *Continental Shelf Research*, *66*, 58-72. Retrieved from https://www.sciencedirect.com/science/article/pii/S0278434313002422 doi: https://doi.org/10.1016/j.csr.2013.07.003

Boiteau, R. M., Till, C. P., Coale, T. H., Fitzsimmons, J. N., Bruland, K. W., & Repeta, D. J. (2019). Patterns of iron and siderophore distributions across the california current system. *Limnology and Oceanography*, *64*(1), 376-389. Retrieved from https://aslopubs.onlinelibrary.wiley.com/doi/abs/10.1002/lno.11046 doi: https://doi.org/10.1002/lno.11046

Bundy, R. M., Abdulla, H. A., Hatcher, P. G., Biller, D. V., Buck, K. N., & Barbeau, K. A. (2015). Iron-binding ligands and humic substances in the san francisco bay estuary and estuarine-influenced shelf regions of coastal california. *Marine Chemistry*, *173*, 183-194. Retrieved from https://www.sciencedirect.com/science/article/pii/S0304420314002199 (SCOR WG 139: Organic Ligands – A Key Control on Trace Metal Biogeochemistry in the Ocean) doi: https://doi.org/10.1016/j.marchem.2014.11.005

Bundy, R. M., Barbeau, K. A., Carter, M., & Jiang, M. (2016). Iron-binding ligands in the

southern california current system: mechanistic studies [Journal Article]. *Frontiers in Marine Science*, *3*. Retrieved from http://www.frontiersin.org/Journal/Abstract.aspx?s=1508&name=marine_biogeochemistry&ART_DOI=10.3389/fmars.2016.00027 doi: 10.3389/fmars.2016.00027

Bundy, R. M., Biller, D. V., Buck, K. N., Bruland, K. W., & Barbeau, K. A. (2014). Distinct pools of dissolved iron-binding ligands in the surface and benthic boundary layer of the california current. *Limnology and Oceanography*, *59*(3), 769-787. Retrieved from https://aslopubs.onlinelibrary.wiley.com/doi/abs/10.4319/lo.2014.59.3.0769 doi: https://doi.org/10.4319/lo.2014.59.3.0769

Chase, Z., Johnson, K. S., Elrod, V. A., Plant, J. N., Fitzwater, S. E., Pickell, L., & Sakamoto, C. M. (2005). Manganese and iron distributions off central california influenced by upwelling and shelf width. *Marine Chemistry*, *95*(3), 235-254. Retrieved from https://www.sciencedirect.com/science/article/pii/S0304420304002506 doi: https://doi.org/10.1016/j.marchem.2004.09.006

Chase, Z., van Geen, A., Kosro, P. M., Marra, J., & Wheeler, P. A. (2002). Iron, nutrient, and phytoplankton distributions in oregon coastal waters. *Journal of Geophysical Research: Oceans*, *107*(C10), 38-1-38-17. Retrieved from https://agupubs.onlinelibrary.wiley.com/doi/abs/10.1029/2001JC000987 doi: https://doi.org/10.1029/2001JC000987

Elrod, V. A., Johnson, K. S., Fitzwater, S. E., & Plant, J. N. (2008). A long-term, high-resolution record of surface water iron concentrations in the upwelling-driven central california region. *Journal of Geophysical Research: Oceans*, *113*(C11). Retrieved from https://agupubs.onlinelibrary.wiley.com/doi/abs/10.1029/2007JC004610 doi: https://doi.org/10.1029/2007JC004610

Feely, R. A., Alin, S. R., Carter, B., Bednaršek, N., Hales, B., Chan, F., ... others (2016). Chemical and biological impacts of ocean acidification along the west coast of north america. *Estuarine, Coastal and Shelf Science*, *183*, 260–270.

Firme, G. F., Rue, E. L., Weeks, D. A., Bruland, K. W., & Hutchins, D. A. (2003). Spatial and temporal variability in phytoplankton iron limitation along the california coast and consequences for si, n, and c biogeochemistry. *Global Biogeochemical Cycles*, *17*(1). Retrieved from https://agupubs.onlinelibrary.wiley.com/doi/abs/10.1029/2001GB001824 doi: https://doi.org/10.1029/2001GB001824

Fitzwater, S. E., Johnson, K. S., Elrod, V. A., Ryan, J. P., Coletti, L. J., Tanner, S. J., ... Chavez, F. P. (2003). Iron, nutrient and phytoplankton biomass relationships in upwelled waters of the california coastal system. *Continental Shelf Research*, *23*(16), 1523-1544. Retrieved from https://www.sciencedirect.com/science/article/pii/S0278434303001481 doi: https://doi.org/10.1016/j.csr.2003.08.004

Garcia, H., Locarnini, R., Boyer, T., Antonov, J., Baranova, O., Zweng, M., & Johnson, D. (2009). Dissolved oxygen, apparent oxygen utilization, and oxygen saturation. *World ocean atlas*, *3*.

Hogle, S. L., Dupont, C. L., Hopkinson, B. M., King, A. L., Buck, K. N., Roe, K. L., ... Barbeau, K. A. (2018). Pervasive iron limitation at subsurface chlorophyll maxima of the california current. *Proceedings of the National Academy of Sciences*, *115*(52), 13300-13305. Retrieved from https://www.pnas.org/doi/abs/10.1073/pnas.1813192115 doi: 10.1073/pnas.1813192115

John, S. G., Mendez, J., Moffett, J., & Adkins, J. (2012). The flux of iron and iron isotopes from san pedro basin sediments. *Geochimica et Cosmochimica Acta*, *93*, 14-29. Retrieved

from https://www.sciencedirect.com/science/article/pii/S0016703712003547 doi: https://doi.org/10.1016/j.gca.2012.06.003

Johnson, K. S., Chavez, F. P., Elrod, V. A., Fitzwater, S. E., Pennington, J. T., Buck, K. R., & Walz, P. M. (2001). The annual cycle of iron and the biological response in central california coastal waters. *Geophysical Research Letters*, *28*(7), 1247-1250. Retrieved from https://agupubs.onlinelibrary.wiley.com/doi/abs/10.1029/2000GL012433 doi: https://doi.org/10.1029/2000GL012433

Johnson, K. S., Elrod, V. A., Fitzwater, S. E., Plant, J. N., Chavez, F. P., Tanner, S. J., ... Karl, D. M. (2003). Surface ocean-lower atmosphere interactions in the northeast pacific ocean gyre: Aerosols, iron, and the ecosystem response. *Global Biogeochemical Cycles*, *17*(2). Retrieved from https://agupubs.onlinelibrary.wiley.com/doi/abs/10.1029/2002GB002004 doi: https://doi.org/10.1029/2002GB002004

Kelly, R. L., Bian, X., Feakins, S. J., Fornace, K. L., Gunderson, T., Hawco, N. J., ... John, S. G. (2021). Delivery of metals and dissolved black carbon to the southern california coastal ocean via aerosols and floodwaters following the 2017 thomas fire. *Journal of Geophysical Research: Biogeosciences*, *126*(3), e2020JG006117. Retrieved from https://agupubs.onlinelibrary.wiley.com/doi/abs/10.1029/2020JG006117 (e2020JG006117 2020JG006117) doi: https://doi.org/10.1029/2020JG006117

King, A. L., & Barbeau, K. A. (2011). Dissolved iron and macronutrient distributions in the southern california current system. *Journal of Geophysical Research: Oceans*, *116*(C3). Retrieved from https://agupubs.onlinelibrary.wiley.com/doi/abs/10.1029/2010JC006324 doi: https://doi.org/10.1029/2010JC006324

Landing, W. M., & Bruland, K. W. (1987). The contrasting biogeochemistry of iron and

manganese in the pacific ocean. *Geochimica et Cosmochimica Acta*, *51*(1), 29-43. Retrieved from https://www.sciencedirect.com/science/article/pii/0016703787900044 doi: https://doi.org/10.1016/0016-7037(87)90004-4

Lohan, M. C., & Bruland, K. W. (2008). Elevated fe(ii) and dissolved fe in hypoxic shelf waters off oregon and washington: An enhanced source of iron to coastal upwelling regimes. *Environmental Science & Technology*, *42*(17), 6462-6468. Retrieved from https://doi.org/10.1021/es800144j (PMID: 18800515) doi: 10.1021/es800144j

Martin, J. H., & Michael Gordon, R. (1988). Northeast pacific iron distributions in relation to phytoplankton productivity [Journal Article]. *Deep Sea Research Part A. Oceanographic Research Papers*, *35*(2), 177-196. Retrieved from http://www.sciencedirect.com/science/article/pii/0198014988900350 doi: http://dx.doi.org/10.1016/0198-0149(88)90035-0

Pelland, N. A., Eriksen, C. C., & Lee, C. M. (2013). Subthermocline eddies over the washington continental slope as observed by seagliders, 2003–09. *Journal of Physical Oceanography*, *43*(10), 2025–2053.

Pierce, S., Smith, R., Kosro, P., Barth, J., & Wilson, C. (2000). Continuity of the poleward undercurrent along the eastern boundary of the mid-latitude north pacific. *Deep Sea Research Part II: Topical Studies in Oceanography*, *47*(5-6), 811–829.

Risien, C. M., Cervantes, B. T., Fewings, M. R., Barth, J. A., & Kosro, P. M. (2023). A stitch in time: Combining more than two decades of mooring data from the central oregon shelf. *Data in Brief*, *48*, 109041.

Severmann, S., McManus, J., Berelson, W. M., & Hammond, D. E. (2010). The continental shelf benthic iron flux and its isotope composition [Journal Article]. *Geochimica et Cosmochimica Acta*, *74*(14), 3984-4004. Retrieved from http://www.sciencedirect.com/science/

article/pii/S0016703710002073 doi: http://dx.doi.org/10.1016/j.gca.2010.04.022

Till, C. P., Solomon, J. R., Cohen, N. R., Lampe, R. H., Marchetti, A., Coale, T. H., & Bruland, K. W. (2019). The iron limitation mosaic in the california current system: Factors governing fe availability in the shelf/near-shelf region. *Limnology and Oceanography*, *64*(1), 109-123. Retrieved from https://aslopubs.onlinelibrary.wiley.com/doi/abs/10.1002/lno.11022 doi: https://doi.org/10.1002/lno.11022

Wong, K. H., Nishioka, J., Kim, T., & Obata, H. (2022). Long-range lateral transport of dissolved manganese and iron in the subarctic pacific. *Journal of Geophysical Research: Oceans*, *127*(2), e2021JC017652. Retrieved from https://agupubs.onlinelibrary.wiley.com/doi/abs/10.1029/2021JC017652 (e2021JC017652 2021JC017652) doi: https://doi.org/10.1029/2021JC017652